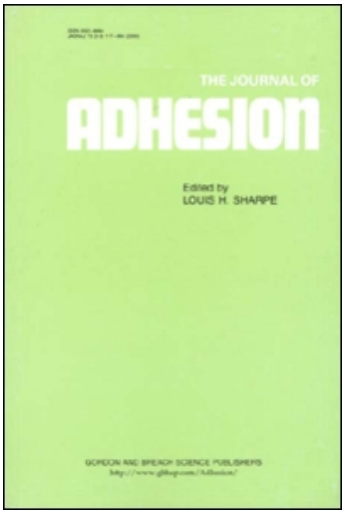

The Journal of Adhesion
Publication details, including instructions for authors and subscription information:
http://www.informaworld.com/smpp/title~content=t713453635

Improved Analytical Models for Mixed-Mode Bending Tests of Adhesively Bonded Joints

Z. Liu[a]; R. F. Gibson[a]; G. M. Newaz[a]
[a] Advanced Composites Research Laboratory, Mechanical Engineering Department, Wayne State University, Detroit, Michigan, USA

Online publication date: 08 September 2010

To cite this Article Liu, Z. , Gibson, R. F. and Newaz, G. M.(2002) 'Improved Analytical Models for Mixed-Mode Bending Tests of Adhesively Bonded Joints', The Journal of Adhesion, 78: 3, 245 — 268
To link to this Article: DOI: 10.1080/00218460210410
URL: http://dx.doi.org/10.1080/00218460210410

The Journal of Adhesion, 78: 245–268, 2002

0021-8464/02 $12.00 +.00

IMPROVED ANALYTICAL MODELS FOR MIXED-MODE BENDING TESTS OF ADHESIVELY BONDED JOINTS

Z. Liu, R. F. Gibson, and G. M. Newaz
Advanced Composites Research Laboratory, Mechanical Engineering Department, Wayne State University, Detroit, Michigan, USA

In this paper, improved analytical models have been developed for more accurate determination of mode I and mode II compliances and strain energy release rates of adhesively bonded Double Cantilever Beam (DCB) type specimens. In these models, the effects of adhesive layer, elastic foundation and shearing deformation ahead of the crack tip due to the Saint-Venant end effect were considered. The improved analytical models were verified using finite element analysis (FEA), and excellent agreements were found for a variety of crack lengths. The comparisons of the measured and predicted testing machine loading point compliances with crack length at three different mixed-mode loading conditions for the adhesive layer thickness of 0.254 mm were also performed for further validation. In addition, contributions to the total mode I strain energy release rate from each effect are summarized.

Keywords: Adhesively bonded joints; Mixed-mode bending test, Adhesively bonded double cantilever beam; Adhesively bonded end-notched flexure beam; Mode I; Mode II; Strain energy release rate

INTRODUCTION

The Mixed Mode Bending (MMB) test fixture for composite delamination testing [1−2] was successfully modified for the study of fracture behavior of adhesively bonded joints with metallic adherends by using modifications of load introduction and a new specimen design [3−4].

Received 8 January 2001; in final form 22 October 2001.

Presented at the 23rd Annual Meeting of the Adhesion Society, Inc., held at Myrtle Beach, South Carolina, USA, 20−23 February 2000.

The authors gratefully acknowledge the financial support of the Ford University Research Program and the technical advice and assistance of Carl Johnson, Matt Zaluzec, John Hill and Kim Lazarz of the Ford Research Laboratory.

Address correspondence to Ronald F. Gibson, Department of Mechanical Engineering, Wayne State University, 5050 Anthony Wayne Drive, Detroit, MI 48202, USA.
E-mail: gibson@eng.wayne.edu

The major advantage of the MMB test is that it simply combines Double Cantilever Beam (DCB) mode I loading and End-Notched Flexure (ENF) mode II loading.

In order to reduce the complexity of tests and Finite Element Analysis (FEA) and to calculate strain energy release rates, analytical models with good accuracy provide many advantages and improve the understanding of fracture behavior of adhesively bonded joints. A comprehensive review on available analytical models of mode I and mode II strain energy release rates of ahesively bonded joints is provided by Liu [4]. The mode I, mode II and mixed-mode fracture toughnesses of adhesively bonded joints have typically been found from analytical models based on beam theory [5–9]. However, most of the analytical models based on beam theory neglect the effects of adhesive layer, elastic foundation and shearing deformation ahead of the crack tip due to the Saint-Venant end effect [5–10], so there is a need for improvements of available analytical models of strain energy release rates of adhesively bonded joints to include such effects.

IMPROVED ANALYTICAL MODELS

In this section, the improved analytical models based on beam theory for the MMB test of adhesively bonded joints will be developed under the assumptions of linear-elastic fracture mechanics (LEFM) and geometrically linearity. As suggested by Reeder and Crews [1], the contributions to the total strain energy release rate associated with mode I and mode II loading are obtained by consideration of the corresponding loadings. The respective mode I and mode II loading components, P_I and P_{II}, are obtained from equilibrium considerations and depend on the applied load, P, according to the expressions derived by Bhashyam and Davidson [11].

$$P_I = P\left(\frac{3c - L}{4L}\right)\left[1 + \frac{(3c_g - L)}{3c - L}\frac{P_g}{P}\right] \tag{1}$$

$$P_{II} = P\left(\frac{c + L}{L}\right)\left[1 + \frac{(c_g + L)}{(c + L)}\frac{P_g}{P}\right] \tag{2}$$

where c, c_g and L are defined in Figure 1. P_g is the gravitational force due to the weight of the lever and is assumed to act at the center of gravity of the lever defined by c_g.

The mode I or mode II component, G_i^m, of strain energy release rate can be determined by the following equation originally suggested by Irwin and Kies [12]:

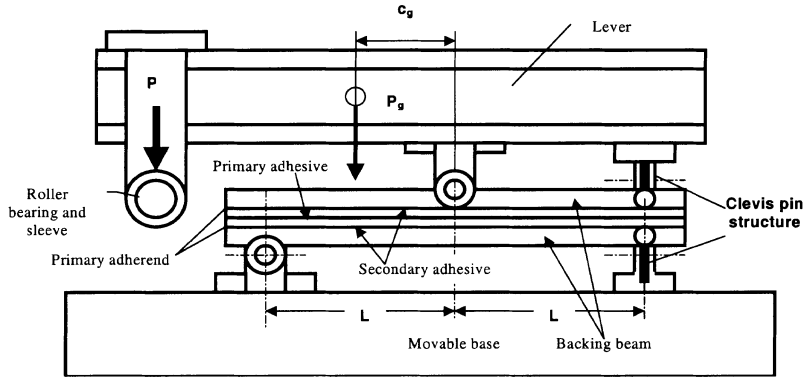

FIGURE 1 Modified MMB test fixture and specimen.

$$G_i^m = \frac{P_i^2}{2B}\frac{\partial C_i^m}{\partial a} \tag{3}$$

where index $i =$ I and II refer to mode I and mode II, respectively. P_i is the corresponding mode loading, C_i^m is the corresponding mode compliance, B is the specimen width, and a is the crack length.

For mixed-mode I and II fracture tests the total energy release rate, G, is given by

$$G = G_I^m + G_{II}^m \tag{4}$$

where G_I^m and G_{II}^m are mode I and mode II components of mixed-mode I and II strain energy release rate, respectively.

Improved Analytical Model for Mode I Strain Energy Release Rate

In this study, a more general and more accurate analytical model for determination of strain energy release rate of an adhesively bonded DCB specimen was developed. In addition to the widely-used beam models which are based on pure bending of the adherend, the improved analytical model integrates the effect of the adhesive layer [13], the elastic foundation effect [14], the Saint-Venant effect [15] and the shear deformation [15–16] into one model, and a more reasonable foundation spring factor and shear correction factor are used. The

model is valid for both isotropic and orthotropic DCB specimens with and without an adhesive layer.

As described above, the total mode I compliance, C_I, of the improved analytical model for the adhesively bonded DCB specimen for Mode I is proposed by the use of the principle of superposition as below:

$$C_I = C_{BS} + C_{EF} + C_{SV} \tag{5}$$

where C_{BS} is the contribution from the Timoshenko model of the cracked part of the adherends, C_{EF} is the contribution from the elastic foundation ahead of the crack tip, and C_{SV} is the contribution from the Saint-Venant end effect.

By using Timoshenko beam theory, the compliance,C_{BS}, of a DCB is approximated by only considering the bending deflection and the deflection due to shear deformation of the cracked part as [16] (Figure 2)

$$C_{BS} = \frac{2\delta_B}{P_I} = \frac{2(\delta_{BB} + \delta_{BS})}{P_I} = \frac{8a^3}{E_F^{\text{adherend}} Bh^3} + \frac{2a}{\mu G_T^{\text{adherend}} Bh} \tag{6}$$

where δ_B is the total deflection of each cracked adherend due to bending and shear deformation, δ_{BB} and δ_{BS} are deflections of the free end of the cracked adherend due to the bending moment and shear force, respectively, μ is the shear correction factor, E_F^{adherend} is the flexural modulus of the adherend, and G_T^{adherend} is the transverse (or through-thickness) shear modulus of the adherend.

However, the support ahead of crack tip is not completely rigid, and transverse translation and rotation actually take place beyond the crack tip. The effect of flexibility at the crack tip in isotropic DCB specimens was first studied by Kanninen [14], who used the Bernoulli-Euler beam model to represent each cracked adherend, and assumed

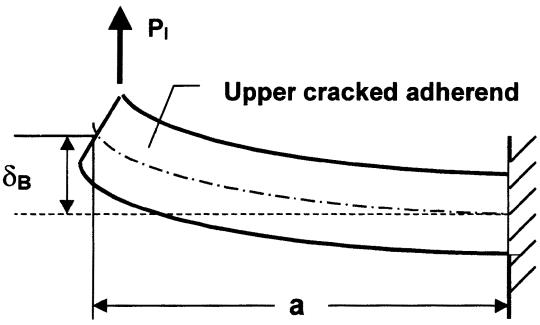

FIGURE 2 Schematic diagram of cantilever beam.

that the uncracked portion is supported by a Winkler foundation consisting of a series of linear springs. Assuming the cracked adherends to be rigid, the load point deformation due to the elastic foundation effect can be divided into two parts by using the Winkler foundation model [14] (Figure 3).

$$\delta_T = \delta_{TT} + \delta_{TR} = \delta_{TT} + \theta_T \mathrm{a} \tag{7}$$

where: δ_{TT} = load point deformation which results from crack tip translation, δ_{TR} = load point deformation which results from crack tip rotation, and θ_T is the rotation angle.

The compliance, C_{EF} for the Winkler foundation is given by [14]

$$C_{EF} = \frac{2\delta_T}{P_I} = \frac{4}{E_F^{\text{adherend}} B \lambda^3 h^3} \left[6\lambda^2 a^2 + 6\lambda a + 3\right] \tag{8}$$

$$\lambda^4 = \frac{K}{4E_F^{\text{adherend}} I} = \frac{3K}{E_F^{\text{adherend}} B h^3} \tag{9}$$

where K = stiffness per unit length of the foundation, and I = the moment of inertia of the adherend.

For adhesively bonded DCB specimens, the effect of the adhesive layer was first considered by Penado based on Kanninen's Winkler foundation model [13]. It was assumed that the uncracked portions of the adherend and the adhesive act as springs in series (Figure 4).

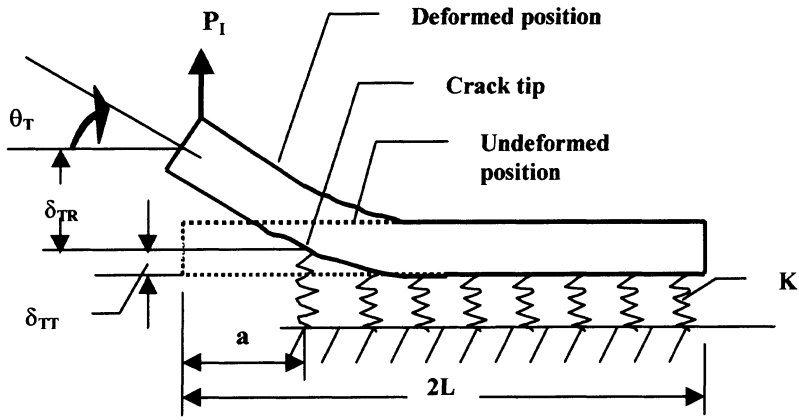

FIGURE 3 Flexural deformation due to transverse compliance in the uncracked part of the DCB.

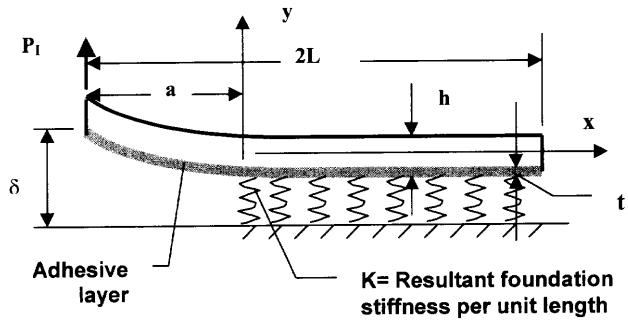

FIGURE 4 Beam on an elastic foundation model including the effect of adhesive layer.

Assuming that K_{adherend} [14] and K_{adhesive} represent the stiffness of the adherend and adhesive, respectively, the resultant foundation stiffness per unit length, K, can be calculated by [13]

$$K = \frac{1}{\frac{1}{K_{\text{adherend}}} + \frac{1}{K_{\text{adhesive}}}} \tag{10}$$

where $K_{\text{adherend}} = E_T^{\text{adherend}} B/(h/2)$, E_T^{adherend} is the transverse modulus of the adherend, and B = the width times one unit length.

For a more general case, the crack plane will be considered at any position, but parallel to the interface between the adherend and the adhesive layer (Figure 5).

An expression for K_{adhesive} can be derived by considering the stress and deformation relations in the adhesive layer [13, 17], and using the Winkler foundation model. Thus, the spring stiffness or elastic foundation modulus of the lower adhesive layer can be expressed as,

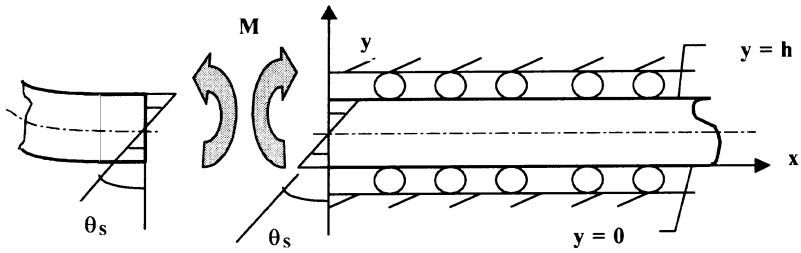

FIGURE 5 Saint-Venant effect in the uncracked part of the DCB.

$$K_{\text{adhesive}} = \frac{B}{2(1-\alpha)t}\frac{E_{\text{adhesive}}}{\left(1-v_{\text{adhesive}}^2\right)} \tag{11}$$

where E_{adhesive} = Young's modulus of adhesive, v_{adhesive} = Poisson's ratio of adhesive, and α is a constant ($0 < \alpha < 1.0$), and $2(1-\alpha)t$ is the thickness of the lower adhesive layer. $\alpha = 0.5$ means that the crack is along the mid-plane of the adhesive layer.

So, the parameter λ in Equation (9) after modification can be rewritten as below,

$$\lambda_U^4 = \frac{K_U}{4E_F^{\text{upper}}I} = \frac{3K_U}{E_F B h^3} \tag{12}$$

where K_U is the resultant elastic foundation modulus for the upper adherend.

Thus, the modified compliance of the upper uncracked adherend is,

$$C_{EF}^{\text{upper}} = \frac{\delta_T}{P_I} = \frac{2}{E_F^{\text{upper}} B \lambda_U^3 h^3}\left[6\lambda_U^2 a^2 + 6\lambda_U a + 3\right] \tag{13}$$

A similar expression of the modified compliance, C_{EF}^{lower}, for the lower uncracked adherend can be obtained by substituting $2\alpha t$ for $2(1-\alpha)t$ in Equation (11). The effective flexural moduli, E_F^{upper} and E_F^{lower} for calculating C_{EF}^{upper} and C_{EF}^{lower} can be estimated by using classical lamination beam theory [18] as below

$$E_F^{\text{upper}} = \frac{1}{(h+2\alpha t)^3}[E_F^{\text{adherend}}(h^3 + 3h^2(2\alpha t) + 3h(2\alpha t)^2) + (2\alpha t)^3 \cdot E_{\text{adhesive}}] \tag{14}$$

E_F^{lower} can be obtained by substituting $2\alpha t$ for $2(1-\alpha)t$ in Equation (14).

Therefore, the total compliance, C_{EF}, of the Winkler foundation for the adhesively bonded DCB specimen including the effect of the adhesive layer can be expressed as

$$C_{EF} = C_{EF}^{\text{upper}} + C_{EF}^{\text{lower}} \tag{15}$$

In the elastic foundation model, the influence of the transverse deformation ahead of the crack tip was analyzed. However, it is obvious that the axial deformations ahead of the crack tip will also affect the crack tip compliance. In order to study this effect, Olsson [15] analyzed the uncracked part of a composite laminated DCB specimen by considering the Saint-Venant effect based on the work of Choi and Horgan [19–20]. In order to isolate this effect, the transverse

modulus was assumed to be nearly infinite, thus, the DCB ahead of the crack tip can be modeled as shown in Figure 5.

The decay length of the Saint-Venant effect, χ, in transversely isotropic materials for both plane strain and generalized plane stress cases is given by the following equation [19–20]

$$\chi = \frac{h}{2\pi}\sqrt{\frac{E_F}{G_T}} \tag{16}$$

where E_F, G_T are the flexural modulus and the transverse shear modulus, respectively, of the composite laminated beam, $E_F \gg E_T$ and $G_T \cong E_T$ or $E_T \gg E_F, G_T$.

The maximum rotation, θ_S, due to the Saint-Venant effect at the crack tip where $x = 0$ (Figure 5) is obtained by using Castigliano's second theorem as

$$\theta_S = \frac{12M\chi}{E_F B h^3} = \frac{12P_I a\chi}{E_F B h^3} \tag{17}$$

The load point deflection of each cracked adherend due to the Saint-Venant effect is given by

$$\delta_S = \theta_S a \tag{18}$$

Therefore, the compliance, C_{SV}, of each uncracked adherend due to the contribution of the Saint-Venant effect is derived as below [15]

$$C_{SV} = \frac{12\chi}{E_F B h}\left(\frac{a}{h}\right)^2 \tag{19}$$

Equations (16)–(19) are derived for a composite beam and are based on the assumption that the crack plane is at the mid-plane of the composite laminated DCB specimen. However, these derivations can be extended to an adhesively bonded DCB specimen with a crack plane at any position parallel to the interface between the adherend and adhesive layer as described before. The compliance for the upper uncracked part is given by

$$C_{SV}^{\text{upper}} = \frac{12\chi}{E_F^{\text{upper}} B(h + 2\alpha t)}\left(\frac{a}{h + 2\alpha t}\right)^2 \tag{20}$$

The lower adherend compliance, C_{SV}^{lower},

$$C_{SV}^{\text{lower}} = \frac{12\chi}{E_F^{\text{lower}} B(h + 2(1-\alpha)t)}\left(\frac{a}{h + 2(1-\alpha)t}\right)^2 \tag{21}$$

and the total compliance of the DCB system due to the Saint-Venant effect is

$$C_{SV} = C_{SV}^{\text{upper}} + C_{SV}^{\text{lower}} \tag{22}$$

When the crack propagates along the mid-plane of the adhesive layer, the total compliance of the DCB system can be expressed as below:

$$C_I = \frac{4}{E_F B \lambda^3 h^3}\left[2\lambda^3 a^3 + 6\lambda^2 a^2 + 6\lambda a + 3\right] + \frac{2a}{\mu G_T^{\text{adherend}} Bh} + \frac{24\chi}{E_F Bh}\left(\frac{a}{h+t}\right)^2 \tag{23}$$

and the corresponding mode I strain energy release rate from Equation (3) is given by

$$G_I = \frac{P_I^2}{2B}\left\{\frac{4}{E_F B(h+t)^3\lambda^3}\left[6\lambda^3 a^2 + 12\lambda^2 a + 6\lambda\right] + \frac{2}{\mu G_T^{\text{adherend}} Bh} + \frac{48\chi a}{E_F B(h+t)^3}\right\} \tag{24}$$

Improved Analytical Model for Mode II Strain Energy Release Rate

The mode II fracture toughness of adhesively bonded ENF specimens was normally determined from Bernoulli-Euler beam theory with shear correction [5], but the effects of the adhesive layer were neglected in the linear elastic analytical models based on beam theory. In order to estimate the strain energy release rate including the nonlinear effects of adhesive in an adhesively bonded ENF specimen under Mode II loading, Chai [21] extended the Goland and Reissner linear-elastic analysis of a lap-shear bonded joint [22] to adhesively bonded ENF specimens. In Chai's work, the effect of adhesive plasticity and the presence of a crack over part of the bondline were incorporated into the estimation of the energy release rate, the adhesive material was modeled as an elastic-perfectly plastic material, and the adherends were assumed to be linear elastic materials. But Chai's model is valid and meaningful only when the shear strain at the crack tip reaches the ultimate shear strain of the adhesive. Prior to that, no crack growth is assumed to take place. Chatterjee [23] also developed a stress analysis including the effects of adhesive layer and adhesive nonlinearity for adhesively bonded ENF specimens. However, no FEA

and experimental verification of the Chai and Chatterjee models has been found in the literature.

In this paper, a more reasonable and more general analytical model for determination of the mode II component of the strain energy release rate for the MMB test and strain energy release rate of adhesively bonded ENF specimen has been developed. The improved linear elastic mechanics of materials model is an extension of previous work by Carlsson and Gillespie [24].

The derivation of the linear elastic mechanics of materials model for mode II strain energy release rate is based on the change of compliance with crack extension. The compliance of the adhesively bonded ENF specimen is defined as the displacement, δ_B, at the central loading point divided by the applied load at the same point, P. With the notations in Figure 6, δB can be calculated from:

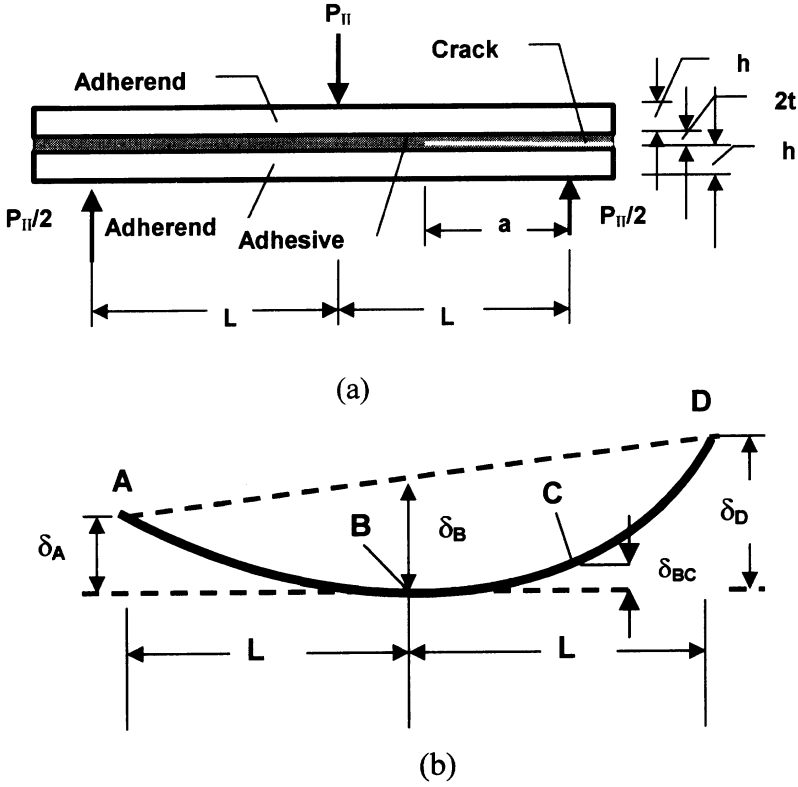

FIGURE 6 Adhesively bonded ENF specimen. (a) Schematic diagram of adhesively bonded ENF specimen; (b) Definition of vertical displacement.

$$\delta_B = \frac{1}{2}(\delta_A + \delta_D) \tag{25}$$

The beams AB and BCD are modeled as cantilever beams with fixity against rotation at point B. No warping is assumed in the cross section at point B due to the approximate symmetry. The effective flexural modulus, E_F, and effective transverse shear modulus, G_T, of the uncracked beam AB can be estimated as below [18]:

$$\frac{1}{G_T} = \frac{1}{G_T^{\text{adherend}}}\left(\frac{h}{h+t}\right) + \frac{1}{G_T^{\text{adhesive}}}\left(\frac{t}{h+t}\right) \tag{26}$$

$$E_F = \frac{1}{(h+t)^3}\left[E_{\text{adherend}}\left(h^3 + 3h^2t + 3ht^2\right) + t^3 \cdot E_{\text{adhesive}}\right] \tag{27}$$

where E_{adherend} = flexural modulus of adherend, E_{adhesive} = Young's modulus of adhesive; G_T^{adherend} and G_T^{adhesive} are transverse shear modulus of adherend and adhesive layer, respectively; h and t are adherend thickness and half-thickness of adhesive layer, respectively.

According to Timoshenko beam theory,

$$\delta_A = \frac{P_{II}L^3}{4E_FB(h+t)^3} + \frac{P_{II}L}{\mu G_TB(h+t)} \tag{28}$$

For the cracked part, CD, the displacement of point D relative to point C has three components. The first is due to the bending and shear deformation, the second is due to the rotation of the cross-section at point C (Figure 6). According the assumptions by Carlsson and Gillespie [24], the upper and lower adherends of the cracked part deform freely under shear loading. Assuming that each cracked adherend carries the same load, $P_{II}/4$, the displacement component due to the first two contributions is given by

$$\delta_{BC} = \frac{P_{II}\left(2L^3 - 3aL^2 + a^3\right)}{8E_FB(h+t)^3} + \frac{P_{II}(L-a)}{4\mu G_TB(h+t)} \tag{29}$$

$$\delta_{CD} = \frac{P_{II}\left(3aL^2 + 5a^3\right)}{8E_F^{\text{adherend}}Bh^3} + \frac{2P_{II}a}{4\mu G_T^{\text{adherend}}Bh} \tag{30}$$

Furthermore, the contribution to the displacement at point D due to the Saint-Venant effect at the crack tip can be expressed as

$$\delta_D^{SV} = \frac{3\chi P_{II}}{E_F^{\text{adherend}}Bh}\left(\frac{a}{h}\right)^2 \tag{31}$$

Therefore, the deflection at point B can be expressed as

$$\delta_B = \delta_{II} = \frac{1}{2}(\delta_A + \delta_D) = \frac{1}{2}\left[\delta_A + \left(\delta_{BC} + \delta_{CD} + \delta_D^{SV}\right)\right] \tag{32}$$

It should be explained that the effect of elastic foundation was not considered for the mode II model due to asymmetric characterization. The compliance of the adhesively bonded ENF specimen is then given by

$$C_{II} = \frac{\delta_{II}}{P_{II}} \tag{33}$$

and the mode II strain energy release rate is obtained by using Equation (3):

$$G_{II} = \frac{1}{2}\frac{P_{II}^2}{2B}\{C_{11} + C_{22}\} + \frac{3\mathrm{P}_{\mathrm{II}}^2\chi a}{B^2 E_F^{\mathrm{adherend}} h^3} \tag{34}$$

with

$$C_{11} = \frac{-3L^2 + 3a^2}{8E_F B(h+t)^3} - \frac{1}{4\mu G_T B(h+t)} \tag{35}$$

$$C_{22} = \frac{3L^2 + 15a^2}{8E_F^{\mathrm{adherend}} Bh^3} + \frac{2}{4\mu G_T^{\mathrm{adherend}} Bh} \tag{36}$$

Verifications of Improved Analytical Models Using FEA

Two-dimensional finite element analysis (FEA) models were constructed to verify the improved analytical models. ABAQUS (version 5.7) was used for the finite element studies. Plane strain conditions were assumed.

Verifications of Improved Mode I Analytical Model

The specimens used for the verification studies were the adhesively bonded DCB specimens with the aluminum alloy adherends and Dow Betamate 4601® epoxy adhesive. All materials were assumed to be linearly elastic and to have invariant, room temperature properties as listed in Table 1 [18].

The adherend thickness was 6.54 mm, and the adhesive thickness was 0.254 mm. Five initial crack lengths were modeled, 50.8 mm, 38.1 mm, 25.4 mm, 12.7 mm and 5.08 mm. The location of the crack was assumed to be in the mid-plane of the adhesive layer.

TABLE 1 Material Properties Used for Mode I Improved Analytical Model and FEA Model

Material	Young's modulus GPa	Poisson's ratio
Adherends (Aluminum alloy 6061)	69.0	0.30
Adhesive (Dow Betamate 4601® epoxy)	3.8	0.36

The specimen was assumed to have a width of 25.4 mm and a length of 100 mm. The applied load was assumed to be 1000 N.

The adhesive layer was modeled using 12 rows of two-dimensional, four-noded bilinear elements (CPE4). The element size was taken from the study of Gillespie *et al.* [24] and Raju *et al.* [25]. The mesh, dimensions, and boundary conditions are shown in Figure 7. Because of symmetry of mode I, only half of the specimen was used for the finite element model. The strain energy release rates were calculated by using the modified crack closure technique [26].

Figures 8 and Figure 9 show the comparisons of the results from the improved analytical model described in Equations (23) and (24) with those from the FEA for mode I strain energy release rates at five different crack lengths. From Figure 8 and Figure 9 it can be seen that the predicted mode I strain energy release rates and loading point deflections from the improved analytical model are in good agreement with those from the FEA model.

In order to understand the contribution of the individual effects described earlier, the predicted contributions of shear deformation, elastic foundation, and Saint-Venant effect as well as bending deformation in the total mode I strain energy release rates of aluminum/epoxy DCB specimens are illustrated in Figures 10 and Figure 11. This is the first time that the relative importance of these four effects has been demonstrated.

Figure 10 and Figure 11 clearly show the importance of considering elastic foundation and Saint-Venant effects as well as shear deformation, which may be significant for short cracks. The inadequacy of the beam models which did not include these effects is also obvious.

Specific conclusions that can be drawn from this investigation are: (1) For the mode I strain energy release rate of adhesively bonded DCB specimens with long cracks, the contributing factors in decreasing order of importance are pure bending, elastic foundation, Saint-Venant effect and shear deformation. (2) For mode I strain energy release rate of adhesively bonded joints with short cracks, the contributing factors in decreasing order of importance are elastic foundation, bending, Saint-Venant effect and shear, (3) The results including the effect of adhesive

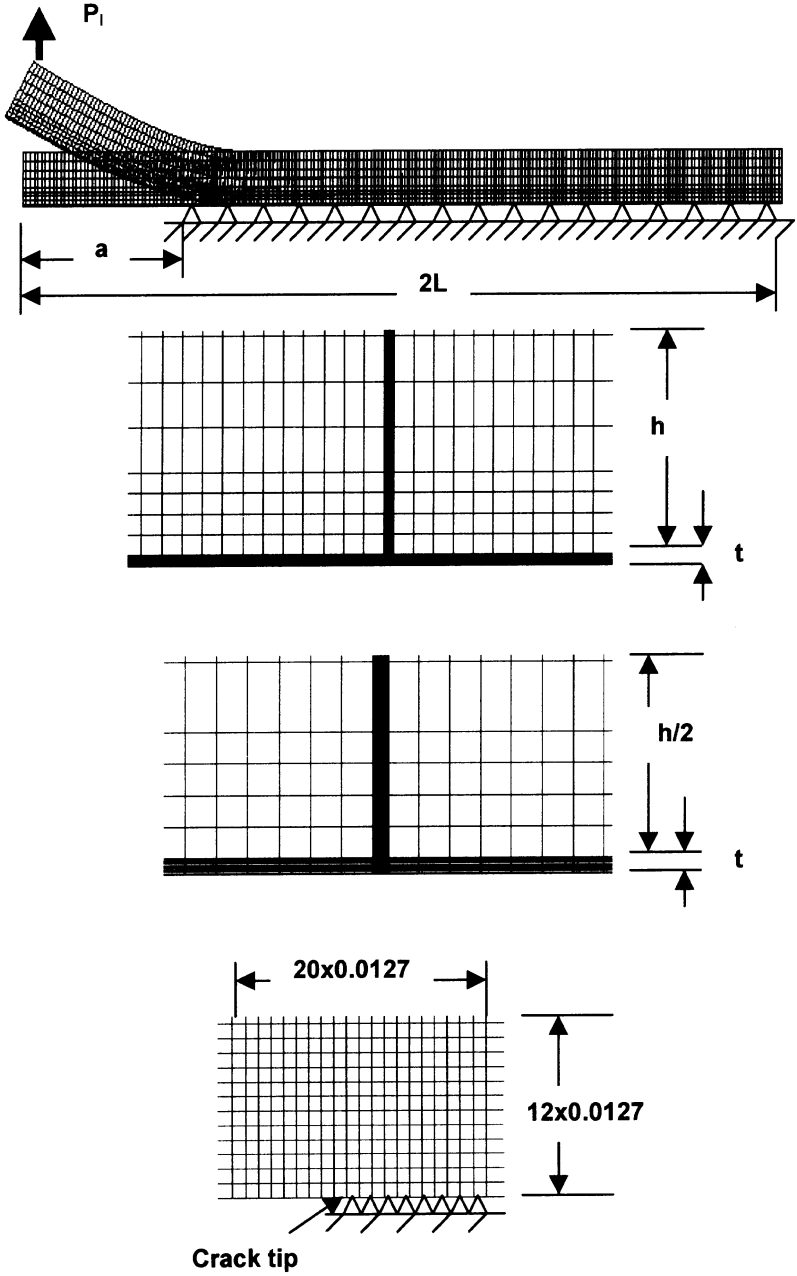

FIGURE 7 Mesh geometry and boundary conditions used in the Finite Element Model for mode I.

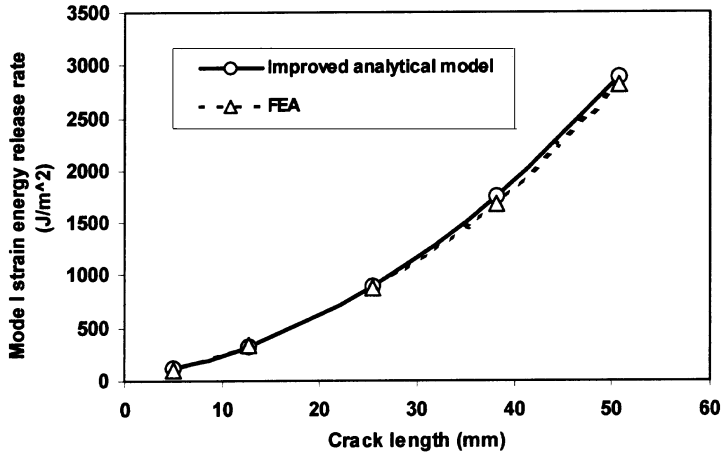

FIGURE 8 Comparison of mode I strain energy release rates from improved analytical model with those from FEA model.

layer and Saint-Venant effects are in good agreement with those of the FEA. (4) The contributions of the effect of elastic foundation, Saint-Venant effects and shear deformation effects to the total Mode I energy release rate increases with decreasing crack length, while the corresponding contribution of pure bending decreases.

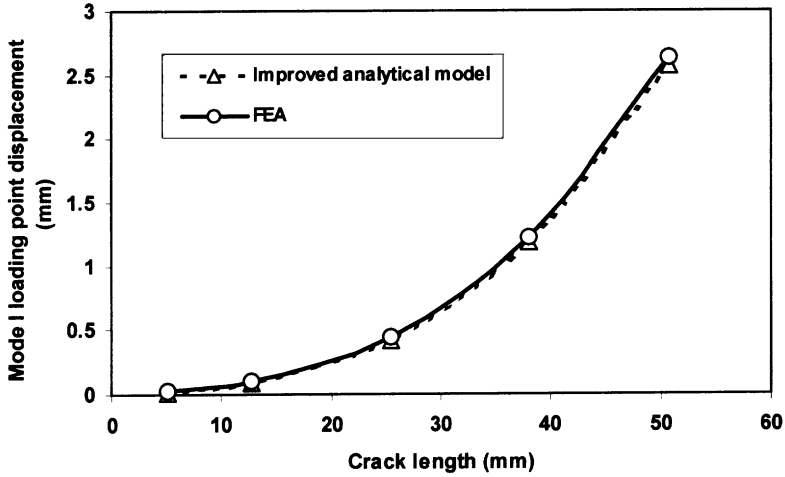

FIGURE 9 Comparison of mode I displacements from improved analytical model with those from FEA model.

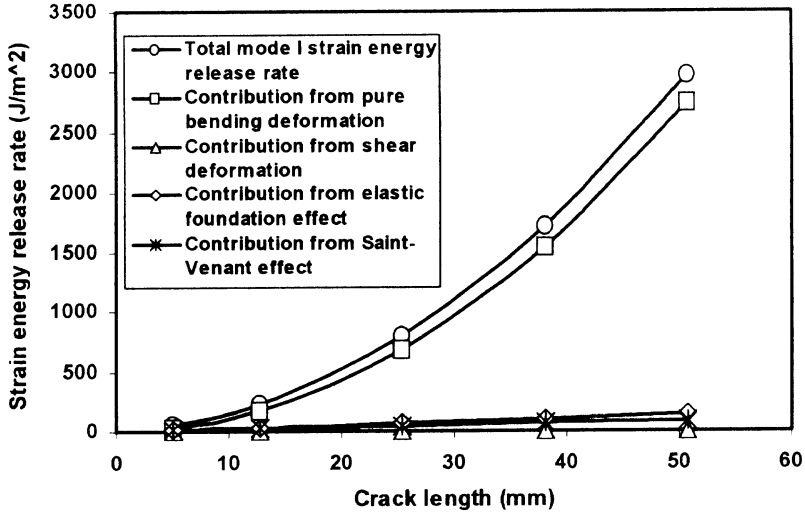

FIGURE 10 Contributions of different effects for mode I strain energy release rate in aluminum/epoxy DCB specimen.

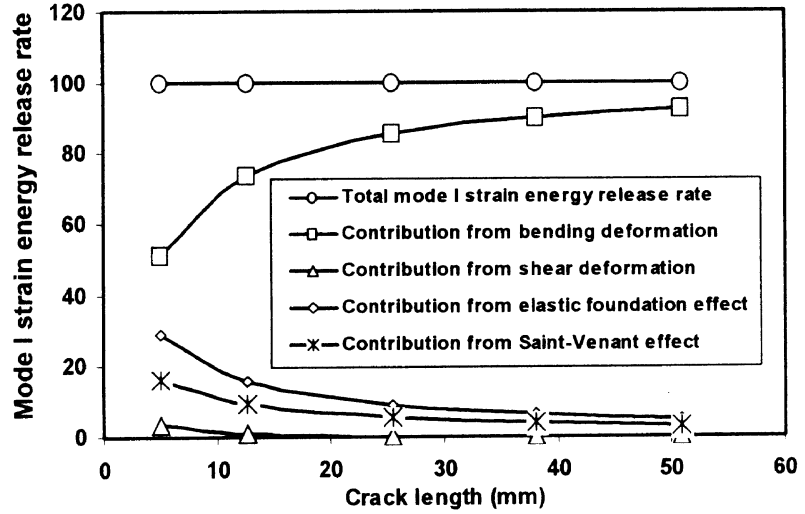

FIGURE 11 Percent contributions of different effects for mode I strain energy release rate in aluminum/epoxy DCB specimen.

Verifications of Improved Mode II Analytical Model

In the FEA models, the material of the adherends was assumed to have linear elastic behavior, while the adhesive material was assumed to have both linear elastic and elastic-perfectly plastic behavior. The yield stress of the adhesive is assumed to be 40.0 MPa.

Steel was chosen as the adherends due to its high stiffness, while the adhesive was a toughened epoxy, Dow Betamate 4601®. All materials were assumed to have invariant, room temperature properties as listed in Table 2. The adherend thickness was 2.0 mm, and the adhesive thickness was 0.2 mm. Three initial crack lengths were modeled, 43.5 mm, 34.0 mm and 22.4 mm. The location of the crack was assumed to be in the mid-plane of the adhesive layer. The specimen was assumed to have a width of 25.4 mm and a length of 120 mm. The applied load was assumed to be 1000 N.

Two-dimensional, eight-noded bilinear elements (CPE8) were used for both the adherends and the adhesive layer. The adhesive layer was modeled using 12 rows. The effect of contact that may develop in the cracked portion of the bond was considered using a built-in contact element in ABAQUS. The Coulomb type friction coefficient was assumed to be 0.1, but it has been shown by Chiang and Chai [27] that the friction coefficient has only a marginal effect. The mesh, dimensions, and boundary conditions are shown in Figure 12. The strain energy release rates were calculated by using the modified closure technique [26].

Figures 13 and Figure 14 show the comparisons of the results from the improved analytical model with those from the FEA model for mode I at three different crack lengths. From Figures 13 and Figure 14 it can be seen that the predicted mode II strain energy release rates and loading point deflections from the improved analytical model are in good agreement with those from the FEA model. However, Chai's model and Chatterjee's model excessively overestimate the mode II strain energy release rates due to the use of idealized linear-perfectly plastic models.

TABLE 2 Material Properties Used for Mode II Improved Analytical Model and FEA Model

Material	Young's modulus GPa	Poisson's ratio	Yield shear stress (MPa)
Adherends (steel)	200.0	0.30	
Adhesive (Betamate 4601®)	3.8	0.36	20.0

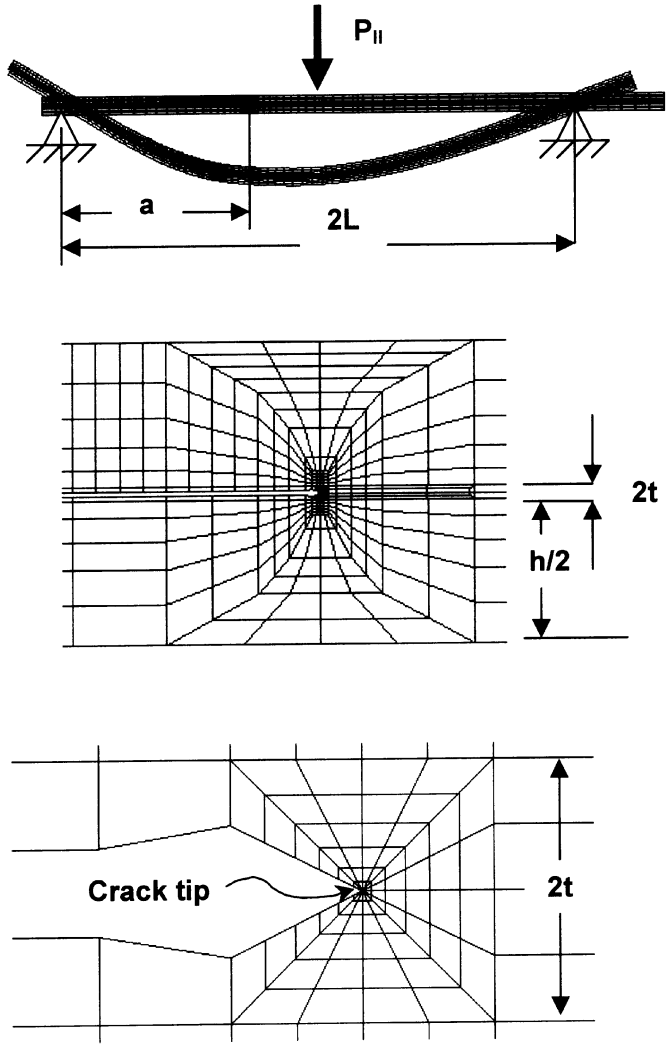

FIGURE 12 Mesh geometry and boundary conditions used in the Finite Element Model for mode II.

Experimental Verification of Analytical Models Using Modified MMB Tests

In order to verify the improved analytical models experimentally, comparisons between measured and predicted compliances at the testing machine loading point were carried out [4].

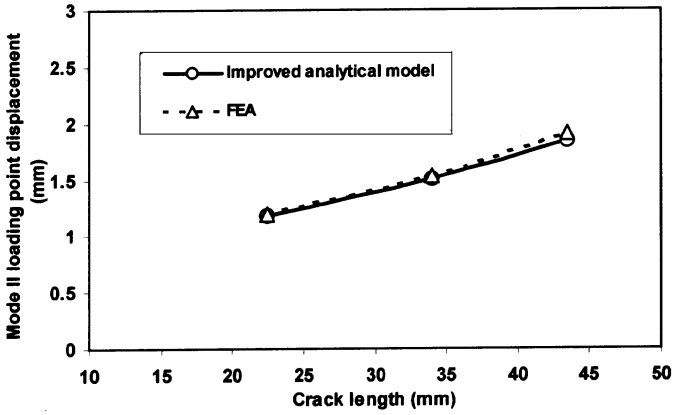

FIGURE 13 Comparison of mode II loading point displacements from improved analytical model with those from FEA model for steel/epoxy ENF specimen.

System Compliance and Measured Testing Machine Loading Point Compliance

Before measuring the testing machine loading point compliance, the compliance of the MMB loading system should be determined at the lever length, c, to be used by exploying steel calibration specimen in

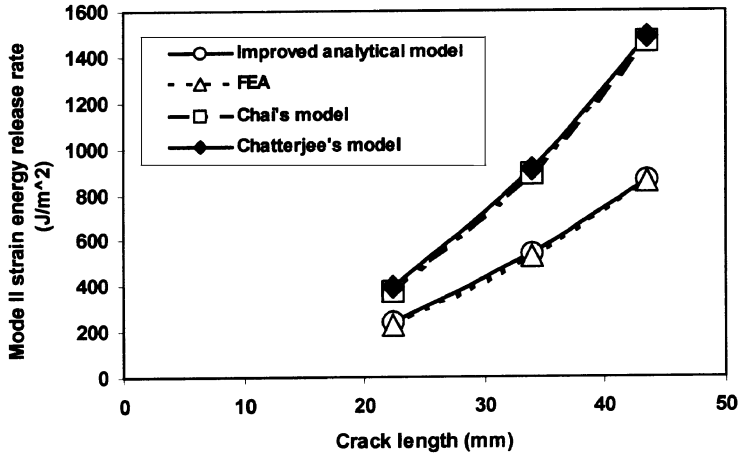

FIGURE 14 Comparison of mode II strain energy release rates from improved analytical model with those from FEA model for steel/epoxy ENF specimen.

the MMB fixture instead of the MMB test specimen (Figure 15). The testing machine loading point (Figure 15) compliance of the calibration specimen including the elastic deformation of the lever can be derived using mechanics of materials and is given by [4]:

$$C_{\text{cal}} = \frac{c^2}{3E_{\text{lever}}I_{\text{lever}}}(L+c) + \frac{2L(c+L)^2}{E_{\text{cal}}B_{\text{cal}}T_{\text{cal}}} \tag{37}$$

where E_{lever} is Young's modulus of the loading lever, I_{lever} is the inertia of moment of the loading lever, E_{cal} is the flexural modulus of the calibration specimen, B_{cal} is the width of the calibration specimen, and T_{cal} is the thickness of the calibration specimen.

The procedure is to load the MMB fixture with the calibration specimen and record the load-displacement history, then measure the slope of the loading curve, m (Figure 16). The testing machine loading point compliance of the MMB test system, C_{sys}, can be calculated using the following equation:

$$C_{\text{sys}} = 1/\text{m} - Ccal \tag{38}$$

Therefore, the measured compliance, C_{mea}, at the loading point after correction is given by

$$C\text{mea} = \frac{\delta_{\text{mea}}}{P} - Csys \tag{39}$$

where δ_{mea} is the displacement at the testing machine loading point.

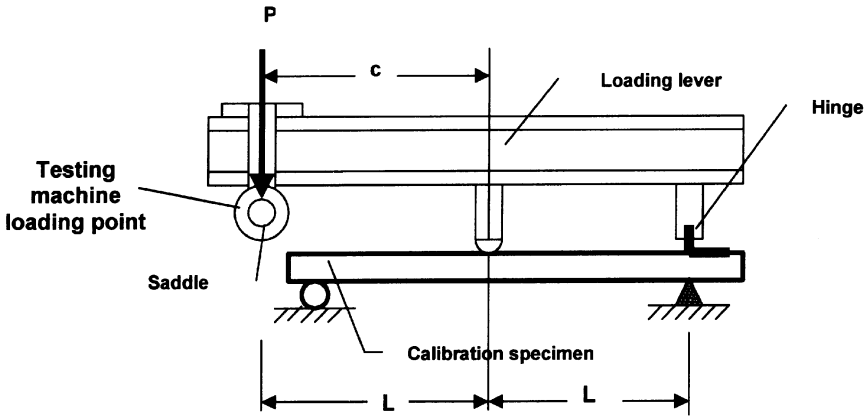

FIGURE 15 Mixed-mode bending test system compliance calibration setup.

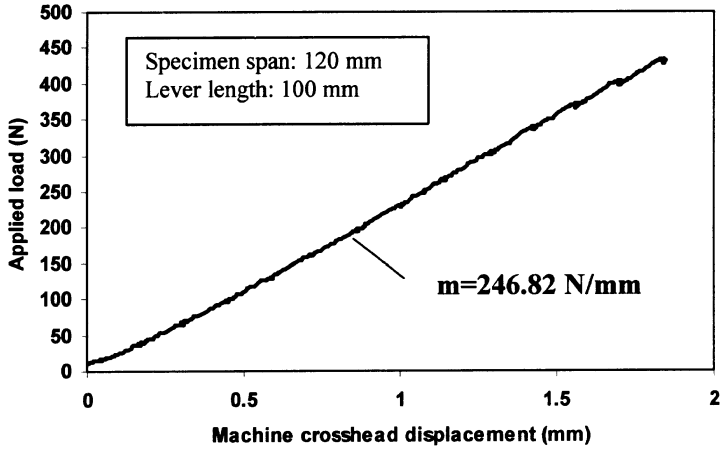

FIGURE 16 Typical MMB test load-displacement curve for testing machine loading point and steel calibration specimen.

Analytical Model for Testing Machine Loading Point Compliance

By using geometric relationships and the principle of superposition, the predicted deflection, δ_P, and compliance, C_P, at the testing machine loading point can be derived as below [4]:

$$\delta_P = \frac{Pc^2}{3E_{\text{lever}}I_{\text{lever}}}(L+c) + \left(\frac{3c-L}{4L}\right)\delta_I + \left(\frac{c+L}{L}\right)\delta_{II} \tag{40}$$

$$C_P = \frac{c^2}{3E_{\text{lever}}I_{\text{lever}}}(L+c) + \left(\frac{3c-L}{4L}\right)^2 C_I + \left(\frac{c+L}{L}\right)^2 C_{II} \tag{41}$$

Comparison of Measured and Predicted Testing Machine Loading Point Compliances

The comparisons of variations of the testing machine loading point compliances with crack length at three different mixed-mode loading conditions for the adhesive layer thickness of 0.254 mm are shown in Figure 17. Although the predicted compliances were slightly less than the measured values, the predicted compliances are still in reasonably good agreement with the measured values, and this gives one additional confidence in the improved analytical models. It should be noted that in the original MMB design Crews and Reeder [1] applied the load

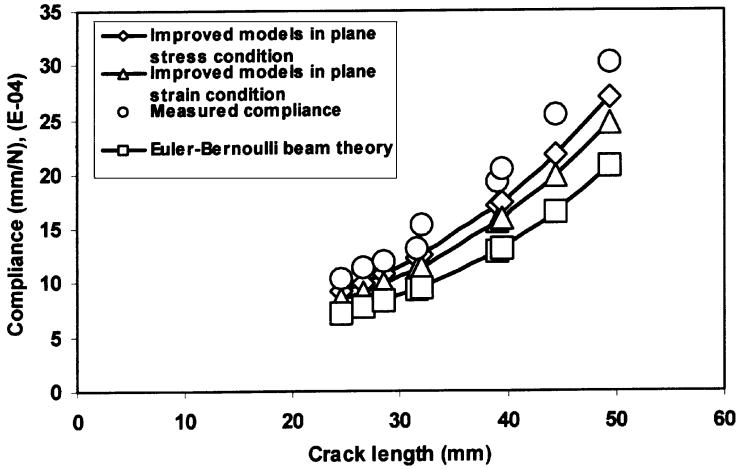

FIGURE 17 Predicted and measured variations of testing machine loading point compliances with crack length for steel calibration specimen.

on the top surface of the lever, which caused excessive loading point rotation, so the test fixture was redesigned [2] by moving the load application point very close to the mid-plane of the specimen through a saddle and yoke arrangement. Although the redesigned MMB fixture reduced the nonlinearity to some degree, some nonlinearity remains [28]. Therefore, it is believed that the measured testing machine loading point compliances are greater than the predicted values because of the geometric nonlinearity in the fixture. As expected, the predicted compliances for the plane strain condition are slightly lower than those for the plane stress condition. The results from the analytical models for mode I and mode II based on the conventional beam theory, Euler-Bernoulli beam theory, are also plotted in Figure 17 for comparison. The improved models show much better agreement with measured values than the conventional Euler-Bernoulli beam model, because the conventional beam model does not consider the effect of the adhesive layer, the Saint-Venant effect, the effect of elastic foundation, and the shear deformation correction.

CONCLUSIONS

In order to make the evaluation of mode I, mode II and mixed-mode I and II strain energy release rates simple and more accurate, improved

analytical models including the effects of the adhesive layer and other corrections to the conventional beam theory have been developed and verified using both FEA and experiments. The only experimental data needed for use of these models are the critical load and the corresponding crack length.

The contributions of individual effects to the total mode I strain energy release rate showed that the use of conventional beam theory is questionable for most of the analytical models in the literature and that the effects of the adhesive layer, the Saint-Venant effect and the effect of elastic foundation must be considered.

REFERENCES

[1] Reeder, J. R. and Crews, Jr., J. H., "Mixed-Mode Bending Method for Delamination Testing," *AIAA Journal*, **28**(7), 1270–1276 (1990).

[2] Reeder, J. R. and Crews, Jr., J. H., "Redesign of the Mixed-Mode Bending Delamination Test to Reduce Non-linear Effects," *J. Composites Technology and Research*, **14**, 12–19 (1992).

[3] Liu, Z. Y., Gibson, R. F., and Newaz, G., "Mixed-Mode Fracture Behavior in Adhesively Bonded Joints," *Proceedings of 23rd Annual Meeting of the Adhesion Society*, Myrtle Beach, SC, pp. 19–21 (2000).

[4] Liu, Z. Y., "Characterization of the Mixed-Mode Fracture Behavior of Adhesively Bonded Metal Joints for Automotive Vehicle Structures," Ph.D. Dissertation, Wayne State University (2000).

[5] Kinloch, A. J., *Adhesion and Adhesives: Science and Technology* (Chapman and Hall, Ltd., London, 1987), pp. 284–290.

[6] Liechti, K. M. and Freda, T., "On the Use of Laminated Beams for the Determination of Pure and Mixed-Mode Fracture Properties of Structural Adhesives," *J. Adhesion*, **29**, 145–169 (1989).

[7] Chai, H., "Experimental Evaluation of Mixed-Mode Fracture in Adhesive Bonds," *Experimental Mechanics*, **32**, 296–303 (1992).

[8] Fernlund, G. and Spelt, J., " Mixed-Mode Fracture Characterization of Adhesive Joints," *Composites Science and Technology*, **50**, 441–449 (1994).

[9] Swadener, J. G., Liechiti, K. M. and Liang, Y. M., "Mixed-Mode Fracture Automotive Bonded Joints," *SAMPE-ACCE-DOE Advanced Composites Conference*, September 27–28, Detroit, 367–370 (1999).

[10] Hutchinson, J. W. and Suo, Z., "Mixed-Mode Cracking in Layered Materials," In: *Advances in Applied Mechanics*, Hutchinson, J. W., Ed., **29**, 63–199 (1992).

[11] Bhashyam, S. and Davidson, B. D., "Evaluation of Data Reduction Methods for the Mixed Mode Bending Test," *AIAA Journal*, **35**(3), 546–552 (1997).

[12] Irwin, G. R. and Kies, J. A., "Critical Energy Release Rate Analysis of Fracture Strength of Large Welded Structures," *Welding Journal*, **33**, 193–198 (1954).

[13] Penado, F. E., "A Closed Form Solution for the Energy Release Rate of the Double Cantilever Beam Specimen with an Adhesive Layer," *J. Composite Materials*, **27**(4), 383–407 (1993).

[14] Kanninen, M. F., "An Augmented Double Cantilever Beam for Studying Crack Propagation and Arrest," *Internat. J. Fracture*, **9**, 83–92 (1973).

[15] Olsson, R., "A Simplified Improved Beam Analysis of the DCB Specimen," *Composites Science and Technology*, **43**(4), 329–338 (1992).

[16] Timoshenko, S. P. and Goodier, J. N., *Theory of Elasticity* (McGraw-Hill, Inc., New York, 1970), pp. 41–46.
[17] Williams, M. L., "The Fracture Threshold for an Adhesive Interlayer," *J. Appl. Polym. Sci.*, **14**, 1121–1126 (1970).
[18] Gibson, R. F., *Principles of Composite Material Mechanics* (McGraw-Hill, Inc., New York, 1994), pp. 192–196.
[19] Horgan, C. O., "On Saint Venant's Principle in Plane Anisotropic Elasticity," *J. Elasticity*, **2**, 169–180 (1972).
[20] Choi, J. and Horgan, C. O., "Saint Venant's Principle and End Effects Anisotropic Elasticity," *J. Appl. Mechanics*, **44**, 424–430 (1977).
[21] Chai, H., "Micromechanics of Shear Deformation in Cracked Bonded Joints," *Internat. J. Fracture*, **58**, 223–239 (1992a).
[22] Goland, M. and Reissner, E., "The Stresses in Cemented Joints, *J. Appl. Mechanics*, **7**, A17–A27 (1944).
[23] Chatterjee, S. N., "Analysis of Test Specimens for Interlaminar Mode II Fracture Toughness: Part II. Effects of Adhesive Layers and Material Nonlinearities," *J. Composite Materials*, **25**, 494–511 (1991).
[24] Carlsson, L. A. and Gillespie, Jr., J. W., "Mode II Interlaminar Fracture of Composites," In: *Application of Fracture Mechanics of Composites*, Friedrich, K., Ed. (Elsevier, Amsterdam, 1989), pp. 113–158.
[25] Raju, I. S., Shivakumar, K. N. and Crews, Jr., J. H., "Three-Dimensional Elastic Analysis of a Composite Double Cantilever Beam Specimen," *AIAA Journal*, **26**(12), 1493–1498 (1988).
[26] Rybicki, E. F. and Kanninen, M. F., "A Finite Element Calculation of Stress Intensity Factors by Modified Crack Closure Integral," *Eng. Fracture Mechanics*, **9**(4), 931–938 (1977).
[27] Chiang, M. Y. M., and Chai, H., "Plastic Deformation Analysis of Cracked Adhesive Bonds Loaded in Shear," *Internat. J. Solids and Structures*, **31**(18), 2477–2490 (1994).
[28] Shivakumar, K. N., Crews, Jr., J. H. and Avva, V. S., "Modified Mixed-Mode Bending Test Apparatus for Measuring Delamination Fracture Toughness of Laminated Composites," *J. Composite Materials*, **32**(9), 804–828 (1998).